

Quantitative Dynamic AFM Hydration-Adsorption Design for Hygroscopic and Bio-Compatible Polymeric Nanofibers

Willy Menacho, Karina N. Catalan, Tomas P. Corrales,* and Horacio V. Guzman*

Nanomechanical properties of bio-compatible polymers play crucial roles in tissue engineering scaffolds and filtration devices. The hygro-mechanical properties of those fibers have been mostly studied from a very coarse perspective, reaching a micrometer-scale. However, at the nanoscale the mechanical response of polymeric fibers becomes more challenging due to both experimental-theoretical limitations. In particular, the environment-mediated mechanical response of polymer-fibers demands advanced models that consider sub-nanometric changes in the local structure of water-intercalated with single-polymer-chains. Herein, atomic force-microscopy (AFM) experiments, analytical theory, and simulations are combined to determine the elastic properties of the nanofibers as a function of relative humidity. The effect of morphological changes from the adsorbed water-layer, and an ensemble of inter-chain interaction strength and morphological changes at peak-forces are explored. For the poly-vinyl-alcohol (PVA) nanofibers, considerable differences are found, which are strongly dependent on the molecular signatures of hydration-adsorption at a polymer-chain level. Here, the semi-empirical model plays a key role in properly interpreting experiments by evaluating only a few observables, the height, phase (dissipation), and alternatively the force-distance curves. Beyond the semi-empirical model, an analytical approach to calculate the peak-forces of hygroscopic materials is featured, which enables on-the-fly characterization of the samples, and thus the interactive adjustment of operational-parameters.

particular, polymers are widely studied systems in soft matter research, due to their physical and chemical properties which can be tuned for different applications, like the design of tissue scaffolds^[5–9] for implants and filtering devices.^[10–12] Despite the multidisciplinary community and reports on nanomechanical properties of polymers with several atomic force microscopy (AFM) techniques,^[13] their hygroscopic properties have been only barely studied. Some topographical swelling measurements have been performed on chitosan,^[14,15] collagen,^[16–18] and wheat macrofibrils.^[19] Recently, Sahin and co-workers studied the hydration properties of bacterial spores, proposing a semi-empirical model for their mechanical properties as they varied with moisture.^[20]

One of the limitations in this regard, is the use of precise experimental settings and optimized cantilevers for performing measurements at different relative humidity (RH), which are mostly designed for either air, vacuum, or liquid environments.^[21–23] Another issue is the correct estimation of forces between the tip and polymer,^[24,25] as well as, tip and environment.^[26,27]


Because of the material's low characteristic energy scales,^[1,2] measuring at higher forces could damage the sample and also bring a wrong interpretation of its nanomechanical parameters.^[28] For example, capillary forces are commonly screened by applying AFM in liquid,^[29] nonetheless, barely explored at variable relative humidities.^[30]

1. Introduction

Nanomechanical properties of soft matter interacting with water are characterized by undergoing significant variations within energy scales close to room temperature (a few $k_B T$ s).^[1–4] In

W. Menacho, H. V. Guzman
Departamento de Física Teórica de la Materia Condensada
Universidad Autónoma de Madrid
Madrid E-28049, Spain
E-mail: horacio.guzman@uam.es

W. Menacho
Departamento de Ingeniería Mecánica
Universidad Técnica Federico Santa María
Valparaíso 2390123, Chile

 The ORCID identification number(s) for the author(s) of this article can be found under <https://doi.org/10.1002/ssstr.202300379>.

© 2024 The Authors. Small Structures published by Wiley-VCH GmbH. This is an open access article under the terms of the Creative Commons Attribution License, which permits use, distribution and reproduction in any medium, provided the original work is properly cited.

DOI: 10.1002/ssstr.202300379

K. N. Catalan
Max Planck Institute for Polymer Research
Ackermannweg 10, Mainz 55128, Germany

K. N. Catalan, T. P. Corrales
Departamento de Física
Universidad Técnica Federico Santa María
Valparaíso 2390123, Chile
E-mail: tomas.corrales@usm.cl

T. P. Corrales
Millenium Nucleus in NanoBioPhysics (NNBP)
Valparaíso 2340000, Chile

H. V. Guzman
Department of Theoretical Physics
Jožef Stefan Institute
Ljubljana SI-1000, Slovenia

From a modeling viewpoint, molecular simulation of biopolymer fibers immersed in water, such as collagen have been performed to understand the mechanical properties like strain and rupture, which also include spontaneous chemical events.^[18,31] Despite the sophistication of those molecular models, the direct interaction between collagen chains and water or variable moisture have not been quantified yet. In other words, the interaction of water molecules and polymer chains that are able to swell may create several water interactions in between the polymer chains,^[2,20,32,33] which is a challenging factor to be explored with AFM at the molecular level. In fact, most models consider interatomic potentials to be fixed for a given material, defined by a force field. Nonetheless, for hygroscopic materials this behavior can also change, given the sensitivity of the constitutive material parameters as a function of the relative humidity, which can be measured by an AFM.^[20,21,34,35] Hence, a proper model for such polymer fibers interacting with water should provide different physical properties, i.e., topography and stiffness sensitivity to relative humidity, which we obtained from AM-AFM measurements. On top of this, the exerted forces on the polymer are not only based on the material itself, but on the dynamics of

the cantilever tip due to changes in the environment. Both are at the same time dependent in the precise AM-AFM operational parameters, like the set-point amplitude and frequency which are directly related to the viscosity (dissipation from the sample).^[36,37] At the same time there is need to probe polymer properties along a certain range of frequencies, as described for non-hygroscopic materials.^[38] However, the structural and mechanical properties of polymers can be drastically influenced by variable relative humidity. The question that arises, and that we will tackle, is if there is an identifiable tip-sample interaction regime where the mechanical properties of hygroscopic polymers can be modeled within the context of AM-AFM. We take into consideration that the polymer is within a single material-phase, and is not experiencing phase-transitions induced by humidity or tip-sample interactions during the AM-AFM measurement. Here, we propose semi-empirical models for hygroscopic materials, by combining AFM's topographical measurements with nanomechanical properties of polyvinyl-alcohol (PVA) at three different humidities (see **Figure 1a**). We define two models: 1) centered on the topographical/morphological interactions, this means we use non-invasive AM-AFM topographical measurements focused

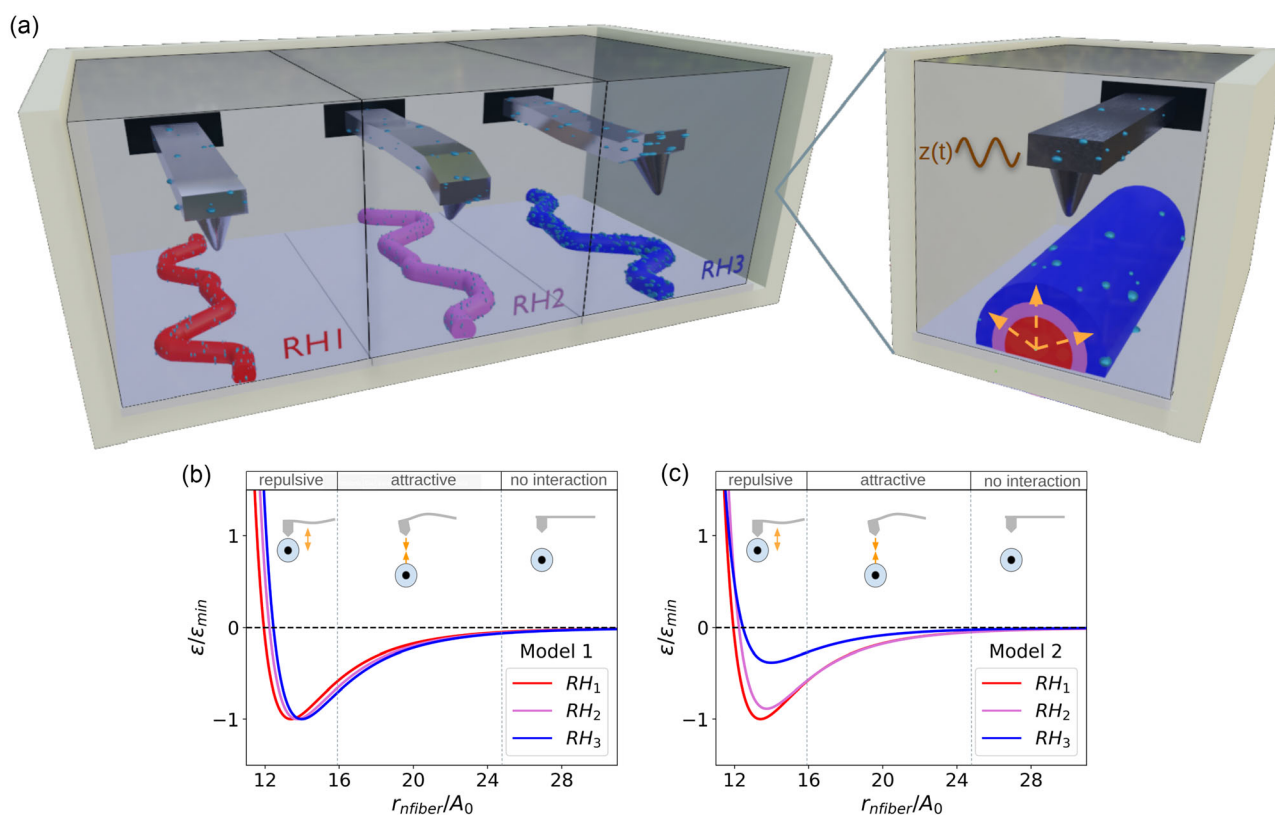


Figure 1. a) Illustration of the PVA fibers at 3 different relative humidity values: 29% (RH_1 in red), 39% (RH_2 in orchid) and 81% (RH_3 in blue). Right-side sketch depicts a nanofiber and the cantilever's oscillatory character with increasing relative humidity. Here, the nanofiber's swelling is represented by orange arrows indicating the growth direction over its cross-section. Modeling of polymeric nanofibers at varying RHs considering a normalized Lennard-Jones potential (ϵ/ϵ_{min}) as a function nanofiber radius, normalized by the free amplitude oscillation of the cantilever (r_{nfiber}/A_0). These models are used to estimate the elasticity values of the nanofibers during swelling. b) Model 1 considers only the topography of the nanofiber as variable, by maintaining the elastic-energy interaction (ϵ), originated by the force-fields of the polymer-water adsorption, constant.^[49,50] c) Model 2 considers topography and elasticity from AFM measurements originated from polymer hydration. The proximity of the bead of chains is also sketched inside figures (b) and (c), showing three regimes of interaction, namely, when the tip is far away (no interaction), attractive and repulsive regimes. The arrows within those regimes show the direction of the force (see more details also in Figure SI, Supporting Information).

only on the topology of the polymer nanofibers (Figure 1b); 2) the second one, also considers elastic energy changes in the polymer nanofibers at the chain level (Figure 1c).

The AM-AFM measurement criteria, are key to estimate the state of the studied material, for example, possible phase transitions, or molecular modifications due to the exerted force from the tip onto the sample. Namely, if a non-invasive measurement mode is employed, then the material can be found in its relaxed state, given a certain constant temperature. Moreover, Tsukruk and co-workers showed that the tip-sample interactions have at least two ways to induce phase-transition, either by increasing the temperature or the loading rate.^[38] In this work, we choose the criteria of the maximum exerted force, which prevents invasiveness of the nanoprobe into soft polymeric samples. However, for the modeling a couple of additional aspects need to be taken into account, such as relaxation times, capillarity, among other, depending on the type of cantilever resonating at different relative humidities.^[25,39–41] Since the phase of the polymer, i.e., rubbery, glassy, or crystalline, is unknown during measurements, the theory can lose its predictability. Hence, we propose two main modeling scenarios; one, which considers the adsorption of water layers on the boundary domains of the sample, and the second which interlaces water and polymer chains. This is particularly important in the case of PVA, which is known to contain both crystalline and amorphous phases in different regions.^[42]

Besides the simulation comparison of both hygroscopic models (regimes), we propose an analytical equation to estimate the peak forces exerted over a viscoelastic material by knowing the operational parameters and phase-shift between tip and sample. This approach considers a sinusoidal piece-wise material

response to the driven oscillating tip in AM-AFM during contact within an oscillation cycle. The material response for a permanent sinusoidal contact of the tip and sample has been previously studied and it has a close dependence on both the deformation (δ), i.e., conservative forces, and the deformation rate ($\delta(\phi)$), i.e., dissipative forces, of polymeric samples.^[36,43–46]

In summary, our semi-empirical models aim to assess polymeric material measurements under different relative humidities. The diverse properties of those materials, make it difficult to interpret measurements at first sight. Hence, we propose two models that tackle the most relevant aspects of hygroscopicity in polymers. Both modeling scenarios illustrate the difference between employing only topography, from our experiments, and combined topography-stiffness values, respectively. This facilitates the theory and also interpretation of the measurements as shown along this work. The two models include the proper sensitive to RH for all interactions, namely, capillary forces, viscosity and electrostatics. In addition, we derive an analytical equation to estimate the peak viscoelastic forces based on the operational parameters and phase shift. Note also that the semi-empirical character of the method refers to experimental measurements at different relative humidities on PVA nanofibers, which to the best of our knowledge are directly compared in this work for the first time.

2. Results

2.1. Identifying Morphological Changes in PVA Nanofibers

Figure 2a shows the AM-AFM topography of PVA nanofibers at 29% (RH_1), 39% (RH_2) and 81% (RH_3) RHs. Figure 2b shows

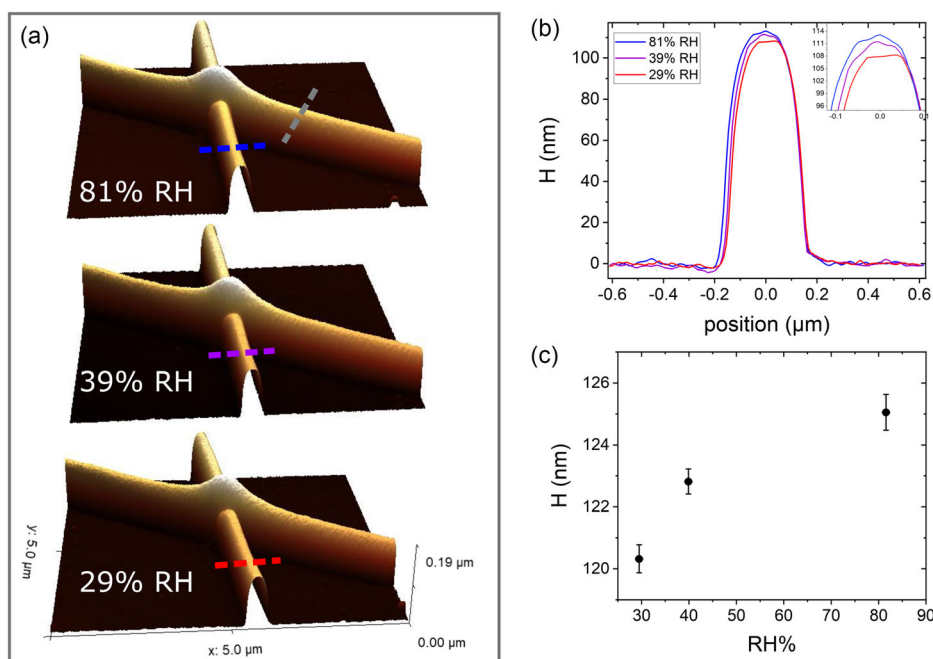


Figure 2. a) 3D topographies of 2 overlapping PVA nanofibers at 29%, 39%, and 81% RH. The dashed-lines indicate the positions where cross-sections are taken and averaged. Red, orchid, and blue are taken on the bottom region of the nanofiber, while the grey dashed-line is taken over the nanofiber's right-side. b) Cross-section of the bottom nanofiber for different humidity values corresponding to the red, orchid, and blue colors of the previous image 1. The inset shows a zoom-in of the profiles as humidity is changed. c) Height of the nanofiber, obtained over three successive images of the same region, averaged from both bottom and right-side cross sections as a function of humidity.

the nanofiber height measurements obtained from cross-sections at the same position along the nanofiber. Figure 2c depicts the reported height values which are obtained by averaging the cross-sections of the three successive images in the same region. The experimental height quantities are employed as inputs for the semi-empirical model, and used in the estimation procedure of the stiffness $\frac{dF_{ts}}{dz}$ S1. In addition to our non-invasive AFM experiments of PVA, the elastic properties of this polymer have been previously measured.^[47,48] The Young moduli values from literature were used for fitting the proposed model 2 (see Figure 1c and S1, Supporting Information). Namely, we consider that the Lennard–Jones (LJ) variable ϵ is obtained based on refs. [47–50], while σ is based on the heights given by Figure 2c. Remarkably, this initial calculation will allow us in the next modeling step to perform dynamic AFM simulations with a RH-dependent Young moduli ($E_s(RH)$). In **Figure 3**, the distribution of the measured phase-shifts are shown for each of the relative humidities (29%, 39%, and 81% RH). The phase-shift distributions quantified in our AFM measurements results from the analysis of two crossing nanofibers as depicted in Figure 3a. The trend in Figure 3b shows for all RHs an increase in the phase-shift as the environment turns more humid. A first interpretation of those results is perfectly understandable from the fact that in AM-AFM a phase-shift $< 90^\circ$ occurs when the interactions turn more repulsive. In particular, at RH 81% we see the population of ϕ at around 43° , such a value decreases to 38° for less humid environments (RH 29%). The numerical counterpart also matches this interpretation, and is provided in the hygroscopic polymers modeling (see Figure 9).

2.2. Modeling Scenarios for Hygroscopic Polymers

Along this work, two models to simulate the PVA response have been considered: model 1 (Figure 1b), employs only the morphological changes from our own measurements, and model 2 (Figure 1c) takes into account morphological and elastic

Table 1. Data used in the simulations shown in Figure 4–10 with an $A_0 = 10$ nm and $A_{sp}/A_0 = 0.8$.^{**} Observe that the quality factor and young's modulus have three different values respectively for $RH_1 = 29\%$, $RH_2 = 39\%$ y $RH_3 = 81\%$, with cantilever model PPP-XYNCSTR-20.^{**} The values presented for quality factor (Q) were calculated at Google Colaboratory notebook Q_calculation, using the method proposed by Sader.^[39,72]

Model	R [nm]	Q^{**}	E_s [MPa]	k [N m ⁻¹]	f [kHz]
1	7	227.32–227.54–228.09	429.21–398.36–377.69	7.4	160
2	7	227.32–227.54–228.09	577.87–475.09–195.20	7.4	160

properties from the the Refs. [47,48]. For both models, **Table 1** shows the resulting elastic moduli as a functions of RH ($E_s(RH)$). Here, we remark that the detailed calculations of elastic moduli as a function of relative humidity are available within the supplementary data of this work.^[51] After defining those moduli for the three tackled RHs, we perform numerical simulations of the tip's motion. The simulation parameters of tip-sample interaction for the measurement of hygroscopic materials are given by the used cantilever (see Table 1) and then the electrostatic, capillary, and van der Waals interactions^[52] are obtained from the literature^[30,40,53] at variable relative humidities, see values summarized in **Table 2**. Note that the specific Q-factors have been obtained experimentally.

In **Figure 4**, one oscillation cycle of the tip-sample forces is shown as a function of time t/T for both models, namely, model 1 shown in Figure 4a–c, and model 2 in the row below Figure 4d–f. For RH_1 and RH_2 , the values of the peak forces for model 2 are higher than model 1, while for RH_3 the opposite relationship is shown. This originates from the strong decreasing tendency of the elastic constant as a function of moisture in model 2, and hence $E_s^{\text{mod1}} > E_s^{\text{mod2}}$ for that specific relative humidity (see Table 1). We quantify each of the calculated forces as shown in Figure S2, Supporting Information, to determine that the strong dependency of the Young moduli on the RH

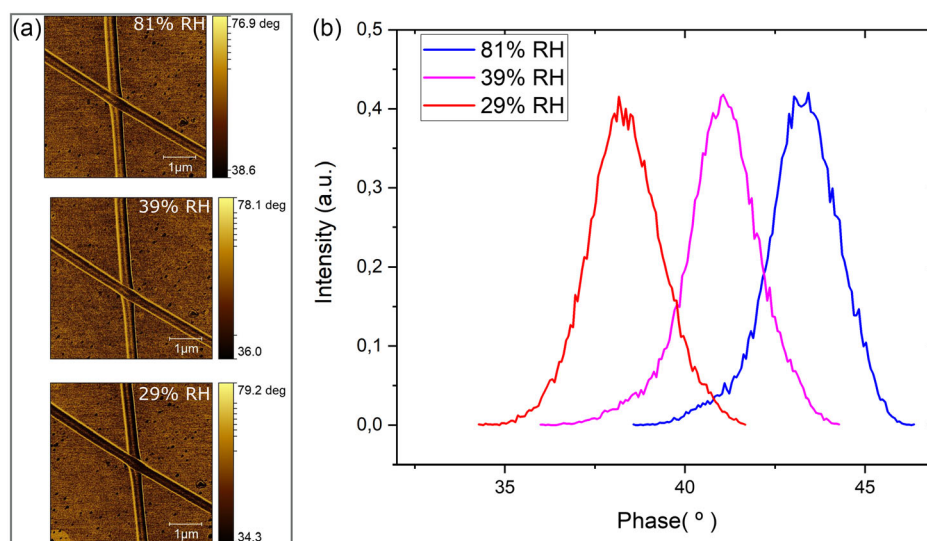


Figure 3. a) Phase-shift images at three different relative humidities: 29% (red), 39% (orchid), and 81% RH (blue). b) Histogram of the nanofibers measured at the same three different relative humidity values described earlier.

Table 2. Data used in the simulations for van der Waals, electrical double-layer, capillary, and viscous forces with H as Hamaker's constant, η as the viscosity coefficient, Γ as the surface energy, ξ_0 as the vacuum permeability, ξ as the relative permeability, χ_s as the surface charge density of the sample, χ_t as the surface charge density of the tip, and λ_D as the Debye length. The values presented for surface energy and capillarity at varying RHs, were calculated at Google Colaboratory notebook SC_calculations.^[30,53,54]

H [10^{-20} J]	η [Pa s]	Γ [mN m $^{-1}$]	ξ_0 [C 2 Nm $^{-2}$]
1	100	1.53–7.68–13.98	8.85
ξ [C 2 Nm $^{-2}$]	χ_s [mC m $^{-2}$]	χ_t [mC m $^{-2}$]	λ_D [nm]
79	16	2.5	1

($E_s(RH)$), as shown in Table 1 determines the behaviour of the peak force for the modeled PVA. On top of this, Figure 4 also shows the dependency of the force on A_{sp} within the range 0.65 to 0.85 A_0 , in steps of 0.01 A_0 . Such a fine grained resolution of A_{sp} allow us also to identify and illustrate in gray dashed curves the maximum dissipative force (See also Figure 6).

After showing the time-domain of our simulations, we pass to the A_{sp} (distance) domain. In the rest of the plots unless explicitly explained, the modeling model 1 will be located on the left hand-side graphs, while model 2 is located on the right hand-side. **Figure 5** shows the peak repulsive forces, by comparing both models we see a clear quantitative difference between model 1 and model 2 for RH_3 . This is originated from the fact that the Young moduli in model 2 has been affected by the assumption that the polymer hydrates by intercalating water molecules within the polymer chains of PVA. A similar behaviour is shown for the dissipative peak forces (**Figure 6**), which for both models show minimum forces (See also Figure 4 curves in gray).

Interestingly the dynamics of the cantilever^[54] can explain those minima, which are not only mechanical-properties dependent, but rather depend on the operational dynamic AFM tip's parameters of Table 2.

The quantitative differences in the peak forces (Figure 5) between the lowest (29%) and the highest (81%) relative humidities are for model 1 always below 100 pN. However for model 2 those difference are around five times the ones of model 1, which show the sensitive character and dependence of mechanical properties of hygroscopic materials. Similar effects are observed for the dissipative peak forces (Figure 6), where model 2 is more sensitive to the RH in terms with a difference of almost 150 pN between highest and lowest RHs. Remarkably, if we subtract the repulsive peak force (Figure 5) and the attractive one (Figure 6), the so called Δ Peak Force is in most cases positive. The exception to the rule is for $A_{sp} > 0.83$ (see Figure 5), which show that the sample could remain in the attractive regime, which is not recommended for measuring polymers in a quantitative way.^[25]

Another relevant quantity in AM-AFM is the maximum indentation, by comparing model 1 and 2 the indentation range is much wider for model 2, almost in 50% (see **Figure 7**). As explained in former works of Guzman et al.^[54,55] the maximum indentation is an indicator of the peak forces and hence the measurement conditions must be adapted to perform non-invasive measurements. Our measurement criteria was to remain above 0.8 A_{sp}/A_0 .

In order to be certain of the AM-AFM operation regime, we show (**Figure 8**) the contact time for both models, showing a generalizable tapping behaviour with contact times between 29% and 17%. Estimating this quantity is also useful to interpret the degree of invasiveness as explained in the literature.^[54,55] In early polymer measurements with AFMs, the characterization of

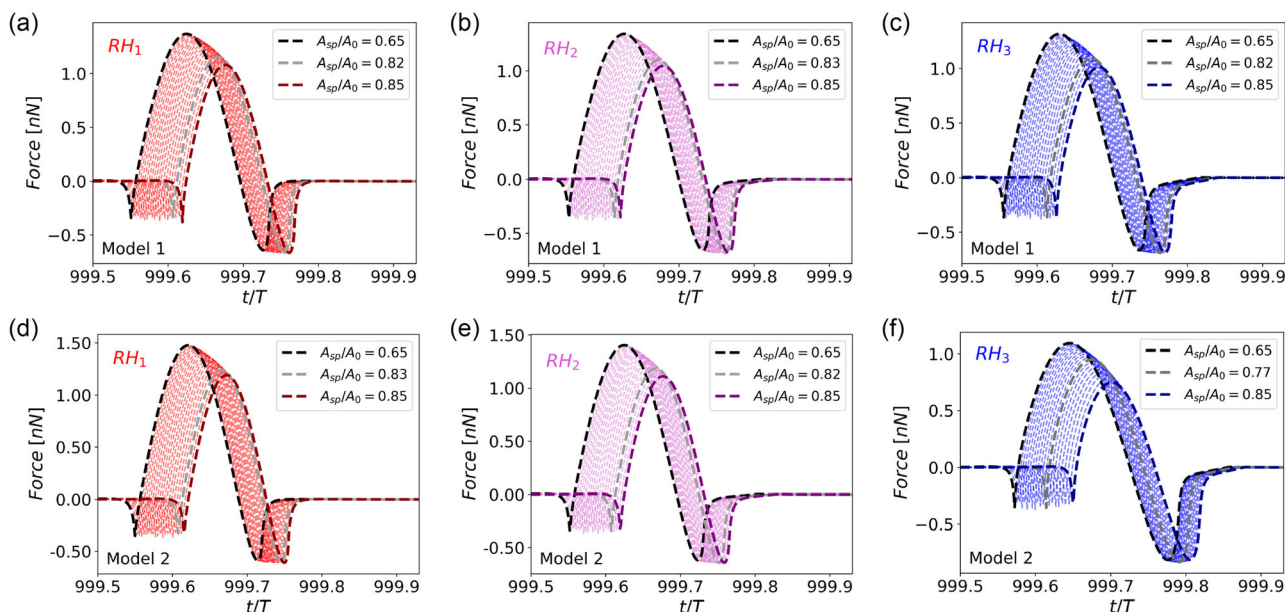


Figure 4. Time-varying tip-sample forces for PVA nanofibers at three different RHs: 29% (RH_1 in red), 39% (RH_2 in orchid), and 81% (RH_3 in blue). The simulations considered viscoelastic, electrostatic, van der Waals, and capillary forces under two modeling scenarios: (a–c) show the curves for model 1; while the curves shown in (d–f) are calculated according to model 2. All plots consider an A_{sp} , in the range from 0.65 to 0.85 A_0 with steps of 0.01 A_0 . The curves in gray illustrate the highest dissipative forces in each relative humidity. Both models employs the simulation parameters described in Table 1 and 2.

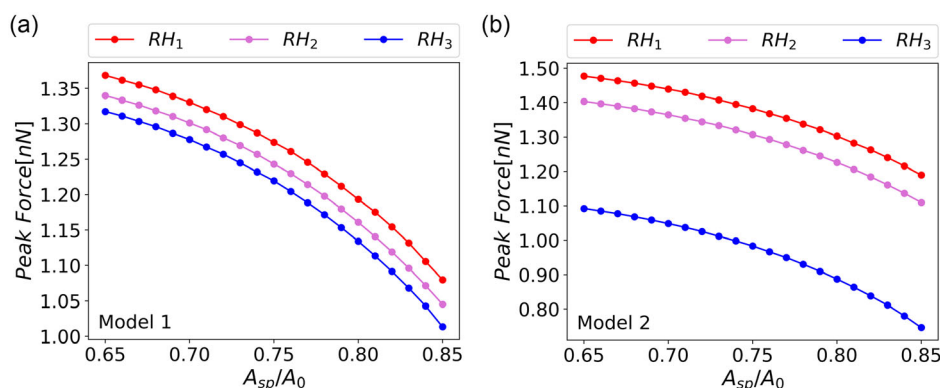


Figure 5. Dependence of the maximum force on the set-point amplitude corresponding to the conditions in: a) Figure 1a model 1, b) Figure 1b model 2. Both models employ the simulation parameters described in Table 1 and 2.

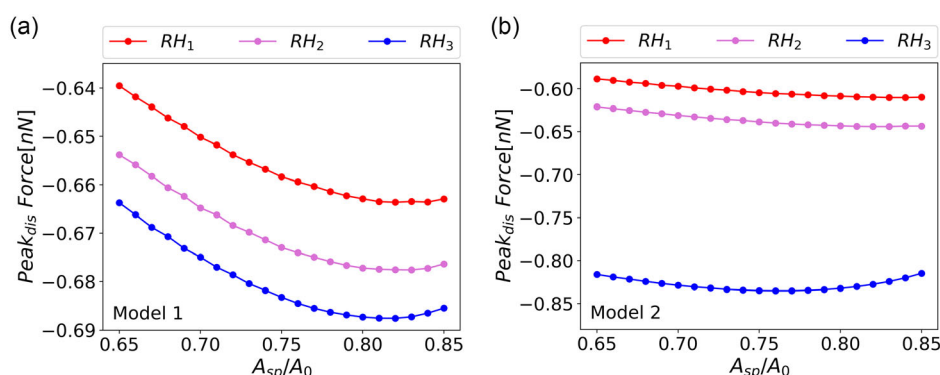


Figure 6. Dissipative force as a function of the set-point amplitude, corresponding to the conditions in: a) Figure 1a model 1, b) Figure 1b model 2. Both models employ the simulation parameters described in Table 1 and 2.

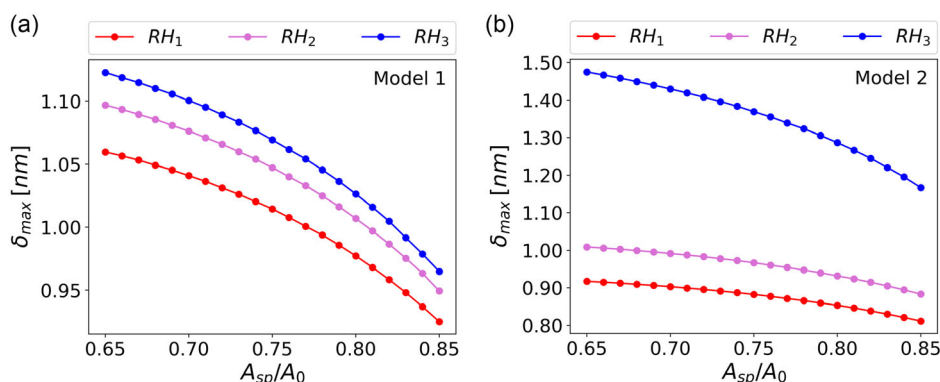


Figure 7. Maximum deformation as a function of the set-point amplitude corresponding to the conditions in: a) Figure 1a model 1, b) Figure 1b model 2. Both models employ the simulation parameters described in Table 1 and 2. Both models employ the simulation parameters described in Table 1 and 2.

viscous properties were an advanced topic.^[56] Currently, the viscosity of soft samples is key to understand their diverse behavior.^[25] The AFM observable to do so is the phase-shift (ϕ), closely related to the physics of energy dissipation,^[52] and hence viscosity.^[54,57–59] In Figure 9, we represent the phase-shift (ϕ) as a function of A_{sp} for both models. The main difference among

them arises at the phase value at 80% of RH, where ϕ reaches a difference of almost 15°. The comparison with our experimental results shown in Figure 3b, turns into a better qualitative agreement model 1 (see Figure 3a). Despite the fact that the phase-shift (ϕ) is a current basic observable in AM-AFM, it is crucial in our modeling analysis of hygroscopic polymers, because it

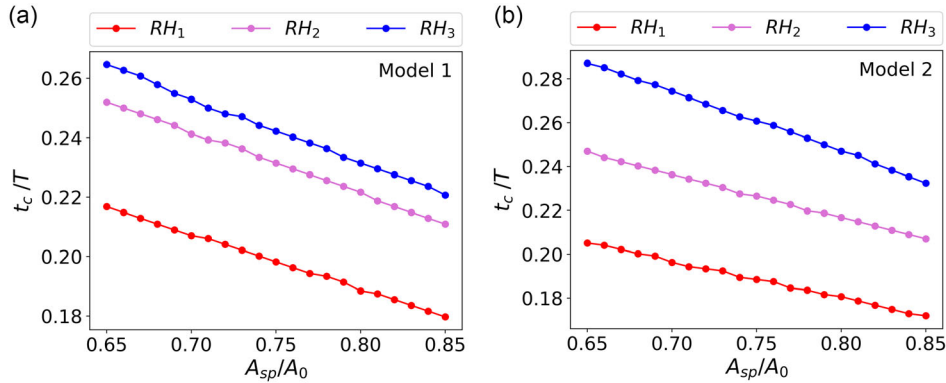


Figure 8. Contact time as a function of the set-point amplitude corresponding to the conditions in: a) Figure 1a model 1, b) Figure 1b model 2. Both models employ the simulation parameters described in Table 1 and 2.

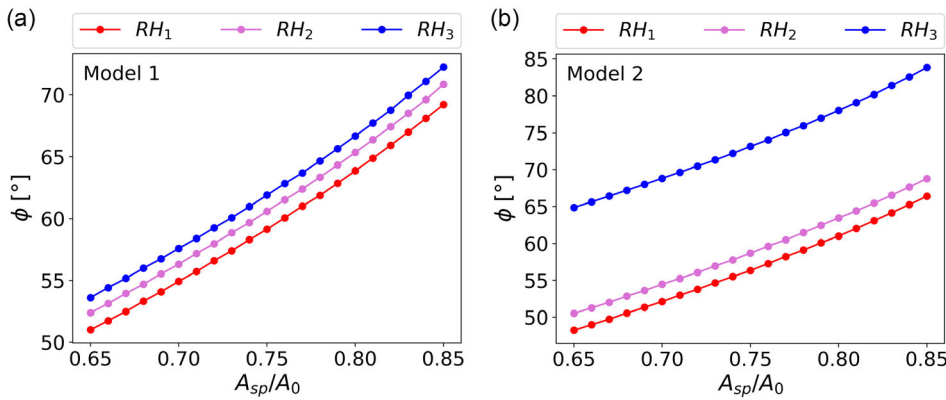


Figure 9. Phase contrast versus set-point amplitude for: a) Figure 1a model 1, b) Figure 1b model 2. Both models employ the simulation parameters described in Table 1 and 2.

is a key factor for choosing a proper model of the relationship ($E_s(RH)$). Thus, helping to identify if water remains adsorbed at the interface or hydrates the polymer chains.

2.3. Derivation of an Analytical Equation to Estimate the Peak Interaction Forces

By combining elastic and viscous forces and assuming that the piece-wise indentation cycles of the AM-AFM tip are periodic, we developed a rapid analytical equation to estimate the peak viscoelastic forces, which are insightful when measuring polymeric samples.^[25] The force term $F(t)$ can be expressed as: $F(t) = F_{\text{peak}}(\omega_c)\cos(\omega_c t - \beta(\omega_c))$, $d(t) < 0$, expanding the cosine term: $F(t) = F_{\text{sto}}(\omega_c)\cos(\omega_c t) + F_{\text{loss}}(\omega_c)\sin(\omega_c t)$, $d(t) < 0$, where $F_{\text{sto}}(\omega_c) = F_p(\omega_c)\cos(\beta(\omega_c))$ is the instantaneous force in phase with the deformation, and $F_{\text{loss}}(\omega_c) = -F_p(\omega_c)\sin(\beta(\omega_c))$ is the instantaneous force out of phase 90° with the deformation.

Now, the deformation $\delta(t)$ can be expressed as $\delta(t) = \delta_{\text{max}}\cos(\omega_c t)$, $d(t) < 0$, $t \in [0, T_d]$, where δ_{max} is the maximum prescribed deformation and ω_c is the angular frequency of contact, with $f_c = 1/(2t_c)$. Note that the contact time requires two assumptions, first to be able to assure the sample's height recovery in each oscillation, namely, $t_c > \tau$, with τ as the polymer

relaxation/recovery time and second $T_d \geq 2t_c$. In fact, t_c is an AFM observable that often requires to be estimated, and the first assumption for our model, when no precise simulations are available is to use $t_c \approx T_d/2$. In a nutshell, t_c is related to both the material relaxation time τ , which in the case of a Kelvin-Voigt model given by the ratio of both viscoelastic variables η_s/E_s , and also the indentation velocity $\dot{\delta}(t)$, which depends on the driven frequency of the cantilever. The deformation rate can be obtained: $\dot{\delta}(t) = -\omega_c\delta_{\text{max}}\sin(\omega_c t)$, $d(t) < 0$. Based on the harmonic approximation used to solve the point mass model, the following relationship is well known, $z(t) = z_0 + A_{\text{sp}}\cos(\omega_d t - \phi)$. The first derivative of $z(t)$ is defined as: $\dot{z}(t) = -\omega_d A_{\text{sp}}\sin(\omega_d t - \phi)$, where A_{sp} is the working amplitude, ω_d is the driven frequency and ϕ is the phase difference between the excited and response oscillating signals of the microscope.

The deformation (also known as indentation) $\delta(t)$ is defined as $\delta(t) = a_0 - z_c - z(t)$, and therefore $\delta(t) = -\dot{z}(t)$. Then, the following relation is obtained: $\dot{\delta}(t) = \omega_d A_{\text{sp}}\sin(\omega_d t - \phi)$, $d(t) < 0$.

Combining the equations above, we obtain the result for the conservative and dissipative forces

$$F_{\text{sto}}(t) = \frac{4}{3} E_s \sqrt{R_t} \sqrt{\delta_{\text{max}} \cos(\omega_c t) (\delta_{\text{max}} \cos(\omega_c t))}, d(t) < 0 \quad (1)$$

$$F_{\text{loss}}(t) = \eta_s \sqrt{R_t} \sqrt{\delta_{\text{max}} \cos(\omega_c t)} (\omega_d A_{\text{sp}} \sin(\omega_d t - \phi)), d(t) < 0 \quad (2)$$

and the total force as

$$F_p(t) = F_{\text{sto}}(t) + F_{\text{loss}}(t) \quad (3)$$

Note here that the force pre-factors indicate a combination of the Kelvin–Voigt and Hertzian mechanics for this case (assuming a non-invasive interaction of model 1), which can be anytime replaced by the SLS or Maxwell models.

The results for quantification of peak forces for PVA-like nanofibers are shown in **Figure 10**. The peak force reconstruction according to Equation (3) is shown in the green curves, which compares to the A_{sp} of the full lines at the three relative humidities ($RH_1 = 29\%$ in red, $RH_2 = 39\%$ in orchid, and $RH_3 = 81\%$ in blue). The general error is for all cases below 7%, compared to the simulations using model 1. Such an equation enables the AFM researchers to estimate the peak forces with only a few operational parameters (i.e., R_t , A_{sp} , ω_d , and ϕ) and estimations of the mechanical properties. Another possible application of Equation (3), is to perform a rapid parametric analysis, as depicted in the case of A_{sp} (dashed lines). This is very practical, when there is an unknown sample underneath and a range/ranges of operational and/or mechanical properties that need to be explored. It is also worth mentioning that analytically, there is no equation for estimating the peak forces including viscous interactions. Additionally, this model can be further adapted to samples of finite sizes, where derivatives of Hertzian mechanics shall be used, and/or power law models.^[25] Regarding the tip-sample contact geometry, we assumed that the shape of the nanofiber is isotropic, which is aligned to modeling of ($E_s(RH)$) described above. In addition, given the dimensions of the ratio $r_{\text{nanofiber}}/\delta_{\text{max}} \approx 100$ of our measurements, Hertzian mechanics is within such a ratio for a sphere-flat surface approach. Moreover, we have tested Equation (3) with model 2 and found that for much softer materials (less than 200 MPa) the estimations of peak forces through Equation (3) are no longer as good as for model 1 (i.e., errors > 10%). As for other force estimation equations,^[28,60–62] the effects of further nanoscale interaction

forces beside the purely mechanical considered in Equation (1) and (2) take an increasingly important role on the total force, as the Young modulus decreases. Hence, it increments the error of any peak force estimation through Equation (3) referenced to the simulation values. In particular, for the AM-AFM simulations we have performed, the model include the atomic and molecular level forces describing capillarity, electrostatics and vdW effects, as well (See Figure S2, Supporting Information).

3. Discussion

Our results show a quantitative perspective of dynamic AFM experiments performed on hygroscopic materials. In particular, the mechanical characterization of PVA nanofibers at different relative humidities. There are several parameters that feed our model, however, the two main direct observables obtained from AFM experiments are the sample's stiffness and morphology. In this regard, we are able to characterize the average molecular parameters involved in the swelling of PVA by a simple Lennard–Jones based model, that takes into account a humidity-dependent Young's modulus ($E_s(RH)$). This enabled us to hypothesize on the physical origin of the inter-chain interactions within the polymer nanofibers. On one hand, the accumulation of adsorbed water layers would imply minor differences in terms of the AFM peak force (≈ 100 pN). On the other hand, a combination of polymer-chains and with water molecules will affect the distance and their interaction strength will vary, which could produce a fivefold increase in the Δ peak-force values compared to model 1.

In addition, our method can be easily extended, for example, it can be combined with further molecular dynamics simulations via the σ and ϵ , which is useful to obtain a correct parametrization of molecular dynamics force fields. Specially, in the case of explicit water models parametrization.^[63–66] Finally, we have also discussed examples on how the changes in environment, require diverse adjustments in the operational parameters of dynamic AFM. Such analysis is required for the correct interpretation of experiments and also elucidate novel physical properties occurring in hygroscopic materials, for example, driving phase-transitions of polymers based on relative humidity variations.

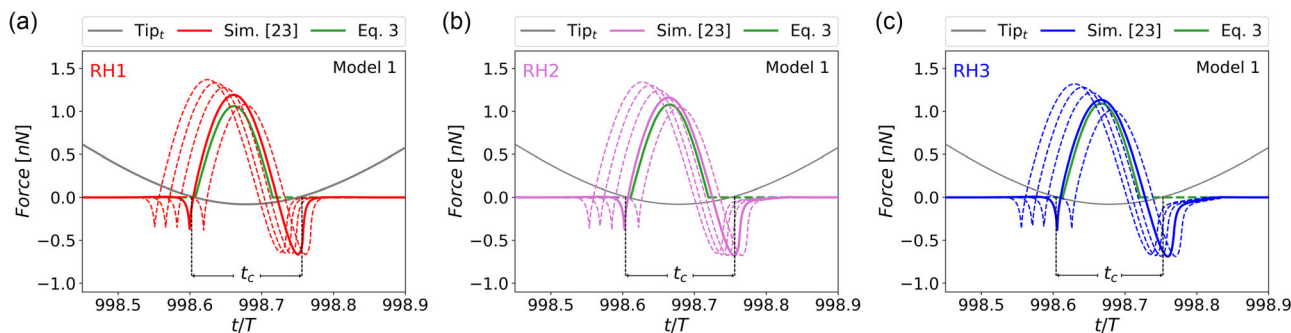


Figure 10. Time-varying force for the PVA nanofibers for three different RHs, namely, a) $RH_1 = 29\%$ in red, b) $RH_2 = 39\%$ in orchid, and c) $RH_3 = 81\%$ in blue. The simulations were performed at five different A_{sp} : 0.65, 0.7, 0.75, 0.8, and 0.85 A_0 . The green curves in all plots show the values obtained from Equation (3) at $A_{\text{sp}} = 0.8 A_0$. The full lines in (a–c) represent the simulations which peak force is closer to the analytical Equation (3) (green curve), and Tip_t represents the AFM tip's trajectory in (gray curves). In all cases the percentile errors between simulations and theory are below 7%. Both models employ the simulation parameters described in Table 1 and 2.

Nevertheless, the simulation of the best operational parameters in the case of dynamic AFM, and cantilever types, can be also tested prior to experiments. By performing simulations in batches of easily *thousands* of simultaneous cases,^[23] if necessary. Note here that those simulations are continuum and hence time-wise very convenient.

Though new exclusive studies for correlating hygroscopic mechanical properties of polymeric PVA nanofibers to the biodegradable^[67,68] activity are necessary in the future, our findings can be fundamental to properly characterize those samples at the nanoscale, by physically understanding in which phase (e.g., glassy or rubbery) the material has been measured and hence how to interpret those data. Moreover, we complement very recent efforts to understanding hygroscopic biological materials like spores,^[20] in these case the model assumes a critical length-scale of the material surrounded by water. However, there are plenty of differences between structures of spores^[20] and polymers that could form crystalline and amorphous regions like PVA. Hence, we propose two modeling scenarios, whereby, the second model will be conceptually similar to the recent theory pioneered by Sahin et al.^[20] Additionally, we would also like to mention that the behavior of polymers at different relative humidities is complex and cannot be entirely explained without understanding fundamental molecular interactions by models at different length and time scales. Hence on top of our pioneering work showing the mechanical properties of PVA nanofibers at three different RHs, future molecular dynamic simulations are also required to evaluate the details of the polymer water force field, and not only in average, the molecular behavior of hygroscopic materials.

4. Conclusion

Based on the integration of AM-AFM imaging and the developed quantitative methodologies, we explored the hygroscopic properties of PVA nanofibers at three different relative humidities. Our findings underline the mechanism of water adsorption onto nanofibers, which explain the major contribution to morphological changes as a function of controlled moisture levels. Furthermore, due to the pioneering character of these characterizations for nanofibers, we hypothesize two different modeling scenarios of water adsorption for polymer chains, allowing the classification of the measurements on different phases of the polymeric nanofiber and more fundamental on the inter-chain polymer chemistry. Comparing the peak forces of both modeling scenarios we report a notorious 5-fold factor difference between both of them. Remark the importance of a proper theoretical interpretation. We estimate the most appropriate scenario as model 1 for our measurements regime, based on the qualitatively comparison of the phase-shift for both modeling scenarios. Those measurements also provide physical evidence for higher dissipation as the ambient moisture increases in polymeric nanofibers, which suggest the need of further developments in viscous models focused on hygroscopic materials. Finally, our findings can pave the way to analyze the biodegradable features of polymer-fibers at the nanoscale, based on the exploration of their nanomechanical properties at different relative humidities. For instance, AFM can capture real-time images of collagen

fibers as they undergo conformational changes, however, the current analysis does not include models accounting for hygroscopicity. The combination of our methods with well-established AFM imaging modes can also contribute in the understanding of biodegradability features at diverse time and length scales. Moreover, our quantitative methodology can assess AFM measurements by exploring ranges of operational conditions and interpreting in which state (rubbery or glassy) our polymer has been sampled. In addition, our approach can be extended for biological hygroscopic materials, which can in principle provide advanced models for systems with functional dual mechanical-regions, like pollen, among others.

5. Experimental and Computational Section

AFM Experiments: The solution used for the synthesis of nanofibers was prepared using: polyvinyl alcohol (PVA) Mw 89 000–98 000, 99+-% hydrolyzed (Sigma-Aldrich, Germany) on aqueous solutions with ultrapure water ($>18.2 \text{ M}\Omega\text{cm}$) (PURELAB Classic ELGA Milli-Q system, France). The solution was made by dissolving 10 wt% PVA in Milli-Q water at 100 °C and was constantly stirred at 350 rpm for 2 h and then the temperature was lowered to 70 °C and it was stirred at 350 rpm for 1 h.

The analyzed sample was synthesized using an in-house electrospinning setup, which was obtained by electrospinning nanofibers onto a small piece ($\approx 1 \text{ cm}^2$) of Silicon Oxide (SiO_2). The SiO_2 was previously cleaned by sonicating the pieces in Ethanol for 15 min and then sonicating again in crystallographic grade Isopropanol for a further 15 min, and then dried with a dry nitrogen flow. The piece of Silicon were attached to a flat aluminum plate, which was connected to a grounded potential. The deposition was carried out by pushing the solution using a New Era Pump Systems Inc. syringe pump, model NE-300 Just Infusion Syringe Pump, at a controlled rate, a disposable 10 mL syringe containing the polymeric solution, which flowed through a 1/8 in. Tygon tube (ramé-hart instrument co.), and which finally ended in the metal syringe with internal diameter of 9 G (ramé-hart instrument co.) located inside the chamber and connected to a high voltage.

The sample was obtained using the following ES parameters: Applied voltage (A.V) = 12 kV, Distance to collector = 10 cm, pump flow = 0.22 mL h^{-1} and exposure time: $<1 \text{ s}$.

To obtain the 3-D topographies of the sample an AFM (hpAFM by Nanomagnetics) coupled to an environmental chamber provided by the same manufacturer, was used. In addition, there was an anti-vibration table by minus-k Technology (model 2000BM-4), on which the entire AFM assembly was supported. The AFM cantilevers used were NANOSENSORS brand, model PPP-XYNCSTR-20 (PointProbe® Plus XY-alignment Non-Contact/Soft Tapping Mode-Reflex Coating) with a resonance frequency of 165 kHz.

To carry out the measurements, a gas injection system was implemented in order to regulate the relative humidity inside the chamber. This system consisted of a dry nitrogen gas line that is divided into two rotameter flow controllers (FL-2516 V, Omega). With one rotameter we controlled the input rate of pure dry nitrogen into the AFM environmental chamber, while the other one regulated the flow of nitrogen injected into Milli-Q water, forming a saturated vapor, which is then out-putted to the AFM chamber. The regulation of the both gas flows is carried out manually with the rotameters. A combination of both gas lines enters the chamber carrying inside a mixture of dry nitrogen and water vapor, which is adjusted to yield the desired RH value. It is possible to measure the humidity in real-time since the environmental chamber has integrated humidity and temperature sensors, which are read from the AFM program and allow to open or close the gas lines depending on the need. It is important to note that environmental AFM chamber had a gas outlet line, so the pressure inside the chamber remains constant before and after the balancing process. Both gas inlet and outlet are sealed when equilibrium has been reached and measurements are in progress. Our humidity control system

allowed us to change this parameter in a range from 20 RH% to 80 RH%. Three AFM images were taken for each humidity value at a same area position, and 7 humidity values were recorded, from 20 to 80 RH% with steps of 10 RH%, which gives us a total of 21 measurements. The average temperature of the measurements was $20^{\circ}\text{C} \pm 1$.

The measurement protocol was as follows: first the sample was placed inside the chamber at room temperature and humidity, the resonance frequency of the AFM cantilever is found and a first measurement AFM image obtained in tapping mode. This imaged region is chosen such that a crossing of 2 nanofibers was located. The rest of the images are recorded over this area in order to establish a reference system from the nanofiber crossing, and ensure accurate positioning. The chamber was closed and the flow of dry nitrogen was turned on until it reached approximately 10 RH% (this took about 8 h), then the system was left to equilibrate for 24 h until it reached the humidity of 20 RH%. After the chamber reaches this value, three successive images are recorded using the same scanning parameters and at the same humidity. Then, the flow of water vapor combined with dry nitrogen was turned on until it increased the humidity by 8 RH%. After reaching the new humidity value, the gas flow was turned off and then we waited 2 h for the humidity to equilibrate inside and finally it reached a value of about 10% over the previous value. Three successive images were recorded and the process was repeated at five more humidity values. The parameters used to obtain all the images were: scanned area = $5 \times 5 \mu\text{m}$, image resolution = 512×512 pixels and scanning speed = $5 \mu\text{m s}^{-1}$. The reported heights of the nanofibers are obtained from cross-sections over the same spot. We measure a distance of $1.2 \mu\text{m}$ from the center of the nanofiber crossing (dashed-lines Figure 2) and average the height of the three successive images for each relative humidity. The average height and standard deviation are obtained using this same procedure.

To proceed in the summary of the data obtained, the values for the heights at a same humidity were averaged (the humidities were also averaged) and the standard deviation of these averages was determined.

AFM Simulations: In the AM-AFM the equation of motion of the cantilever is approximated using the point-mass model^[23,69]

$$\ddot{z}(t) = -\omega_0^2 z(t) - \frac{\omega_0}{Q} \dot{z}(t) + \frac{F_{ts}(d)}{m} + \frac{F_0 \cos(\omega t)}{m} \quad (4)$$

where ω_0 is the angular frequency of resonance, m is the effective mass of the cantilever tip, Q is the quality factor, F_{ts} is the tip-sample resultant force, F_0 is the amplitude, with $\omega_0^2 = \frac{K_c}{m}$ relating the force constant (K_c) of the fundamental resonance (first bending mode) to the effective mass.^[70] The above equation is applicable when the contributions of the higher modes to the cantilever motion are negligible.^[71]

Supporting Information

Supporting Information is available from the Wiley Online Library or from the author.

Acknowledgements

The authors thank Matej Kanduč and Hideki Kobayashi for illuminating discussions on the molecular modeling of PVA. H.V.G. acknowledge financial support from the Slovenian Research Agency ARRS (Funding No. P1-0055) and the Maria Zambrano Grant No. CA6/RSUE/2022-00108 and the recent Ramon y Cajal Grant No. RYC2022-038082-I. H.V.G. and W.M. thank the Red Española de Supercomputación (RES) for the computing time and technical support at the Finisterrae III supercomputer projects FI-2023-1-0029 and FI-2023-2-0036. T.P.C. and H.V.G. acknowledge the support of project Fondecyt Regular 1211901. T.P.C. acknowledges support from ANID by Millennium Science Initiative Program NNBP No. NCN2021-021. K.N.C. acknowledges funding support from a PIICM Scholarship given by UTFSM.

Conflict of Interest

The authors declare no conflict of interest.

Author Contributions

H.V.G. designed the research; H.V.G., T.P.C. and W.M.N. wrote the manuscript. W.M.M. performed the dynamic AFM simulations and static molecular model; K.N.C. performed the AFM experiments; W.M.N., T.P.C. and H.V.G. analyzed and interpreted the data; H.V.G. supervised the research. All authors have read and agreed to the published version of the manuscript.

Data Availability Statement

The data that support the findings of this study are openly available in [Tuning the nanomechanical properties of hygroscopic nanofibers by quantitative multi-step models] at [http://dx.doi.org/10.5281/zenodo.8187354], reference number [8187354].

Keywords

force microscopy, hygroscopic models, nanomechanical properties, polymer nanofibers

Received: September 25, 2023

Revised: December 15, 2023

Published online:

- [1] D. C. Rau, V. A. Parsegian, *Science* **1990**, 249, 1278.
- [2] B. Dünweg, D. Reith, M. Steinhauser, K. Kremer, *J. Chem. Phys.* **2002**, 117, 914.
- [3] C. Peter, K. Kremer, *Faraday Discuss.* **2010**, 144, 9.
- [4] V. Parsegian, T. Zemb, *Curr. Opin. Colloid Interface Sci.* **2011**, 16, 618.
- [5] S. Jekhmene, M. Prachar, R. Pugliese, F. Fontana, J. Medeiros-Silva, F. Gelain, M. Weingarth, *Angew. Chem., Int. Ed.* **2019**, 58, 16943.
- [6] K. N. Catalan, T. P. Corrales, J. C. Forero, C. P. Romero, C. A. Acevedo, *Polymers* **2019**, 11, 4.
- [7] A. Erben, M. Hörning, B. Hartmann, T. Becke, S. A. Eisler, A. Southan, S. Cranz, O. Hayden, N. Kneidinger, M. Königshoff, M. Lindner, G. E. M. Tovar, G. Burgstaller, H. Clausen-Schaumann, S. Sudhop, M. Heymann, *Adv. Healthcare Mater.* **2020**, 9, 2000918.
- [8] G. L. Koons, M. Diba, A. G. Mikos, *Nat. Rev. Mater.* **2020**, 5, 584.
- [9] Y. Song, J. Long, J. P. Dunkers, J. W. Woodcock, H. Lin, D. M. Fox, X. Liao, Y. Lv, L. Yang, M. Y. M. Chiang, *ACS Appl. Mater. Interfaces* **2021**, 13, 58152.
- [10] X. Zhao, Y. Li, T. Hua, P. Jiang, X. Yin, J. Yu, B. Ding, *Small* **2017**, 13, 1603306.
- [11] W. C. K. Poon, A. T. Brown, S. O. L. Direito, D. J. M. Hodgson, L. Le Nagard, A. Lips, C. E. MacPhee, D. Marenduzzo, J. R. Royer, A. F. Silva, J. H. J. Thijssen, S. Titmuss, *Soft Matter* **2020**, 16, 8310.
- [12] A. Božič, M. Kanduč, *J. Biol. Phys.* **2021**, 47, 1.
- [13] A. F. Payam, A. Passian, *Sci. Adv.* **2023**, 9, eadg8292.
- [14] O. Stukalov, C. A. Murray, A. Jacina, J. R. Dutcher, *Rev. Sci. Instrum.* **2006**, 77, 1.
- [15] R. Luna, F. Touhami, M. Uddin, A. Touhami, *Surf. Interfaces* **2022**, 29, 101706.
- [16] E.-c. Spitzner, S. Ro, M. Zerson, A. Bernstein, R. Magerle, *ACS Nano* **2015**, 9, 5683.
- [17] S. Morozova, M. Muthukumar, *J. Chem. Phys.* **2018**, 149, 163333.

- [18] C. Zapp, A. Obarska-Kosinska, B. Rennekamp, M. Kurth, D. M. Hudson, D. Mercadante, U. Barayeu, T. P. Dick, V. Denysenkov, T. Prisner, M. Bennati, C. Daday, R. Kappl, F. Gräter, *Nat. Commun.* **2020**, *11*, 2315.
- [19] F. Terrazas-Valencia, M. Díaz-Ramírez, M. d. I. P. Salgado-Cruz, J. V. Méndez-Méndez, K. I. Toledo-Madrid, G. Calderón-Domínguez, *Micron* **2021**, *143*, 103010.
- [20] S. G. Harrellson, M. S. DeLay, X. Chen, A.-H. Cavusoglu, J. Dworkin, H. A. Stone, O. Sahin, *Nature* **2023**, *619*, 500.
- [21] H. D. Lee, A. V. Tivanski, *Annu. Rev. Phys. Chem.* **2021**, *72*, 235.
- [22] Z. Ying, Z. Zhang, Y. Zhou, Y. Wang, W. Zhang, Q. Huang, Y. Shen, H. Fang, H. Hou, L. Yan, *Sci. Total Environ.* **2022**, *852*, 158441.
- [23] W. Menacho, G. M. R. Ávila, H. V. Guzman, in *Proceedings of the 21st Python In Science Conference* (Eds: M. Agarwal, C. Calloway, D. Niederhut, D. Shupe), Scipy 2023 and Austin, Texas USA **2022** pp. 202–209.
- [24] A. Chandrashekar, P. Belardinelli, M. A. Bessa, U. Staufer, F. Alijani, *Nanoscale Adv.* **2022**, *4*, 2134.
- [25] R. Garcia, *Roy. Soc. Chem.* **2020**, *49*, 5850.
- [26] R. Groth, S. Niazi, G. R. Johnson, Z. Ristovski, *Environ. Sci. Technol.* **2022**, *15*, 10879.
- [27] R. Groth, S. Niazi, K. Spann, G. R. Johnson, Z. Ristovski, *PNAS Nexus* **2023**, *2*, 3.
- [28] H. V. Guzman, *Beilstein J. Nanotechnol.* **2017**, *8*, 968.
- [29] H.-J. Butt, *Biophys. J.* **1991**, *60*, 1438.
- [30] J. L. Pérez-Díaz, M. A. Álvarez Valenzuela, J. C. García-Prada, *J. Colloid Interface Sci.* **2012**, *381*, 180.
- [31] B. Rennekamp, C. Karfusehr, M. Kurth, A. Ünal, D. Monego, K. Riedmiller, G. Gryn'ova, D. M. Hudson, F. Gräter, *Nat. Commun.* **2023**, *14*, 2075.
- [32] S. Kalam, S. A. Abu-Khamsin, M. S. Kamal, S. Patil, *ACS Omega* **2021**, *6*, 32342.
- [33] F. Staniscia, H. V. Guzman, M. Kanduc, *J. Phys. Chem. B* **2022**, *126*, 3374.
- [34] B. R. Neugirg, M. Burgard, A. Greiner, A. Fery, *J. Polym. Sci., Part B: Polym. Phys.* **2016**, *54*, 2418.
- [35] T. U. Rashid, R. E. Gorga, W. E. Krause, *Adv. Eng. Mater.* **2021**, *23*, 2100153.
- [36] S. de Beer, D. van den Ende, F. Mugele, *Nanotechnology* **2010**, *21*, 325703.
- [37] S. de Beer, W. K. den Otter, D. van den Ende, W. J. Briels, F. Mugele, *Tribol. Lett.* **2012**, *48*, 1.
- [38] M. Chyasnavichyus, S. L. Young, V. V. Tsukruk, *Langmuir* **2014**, *30*, 10566.
- [39] C. P. Green, J. E. Sader, *J. Appl. Phys.* **2005**, *98*, 114913.
- [40] B. Rajabifar, J. M. Jadhav, D. Kiracofe, G. F. Meyers, A. Raman, *Macromolecules* **2018**, *51*, 9649.
- [41] A. F. Payam, A. Morelli, P. Lemoine, *Appl. Surf. Sci.* **2021**, *536*, 147698.
- [42] F. Müller-Plathe, P. Bordat, in *Novel Methods In Soft Matter Simulations* (Eds: M. Karttunen, I. Vattulainen, A. Lukkarinen) Volume 640 of Lecture Notes in Physics, Springer, Heidelberg **2004**, pp. 310–326.
- [43] S. N. Magonov, D. H. Reneker, *Annu. Rev. Mater. Sci.* **1997**, *27*, 175.
- [44] N. W. Tschoegl, *The Phenomenological Theory Of Linear Viscoelastic Behavior*, Springer Berlin Heidelberg, Berlin **1989**.
- [45] I. M. Ward, J. Sweeney, *Mechanical Properties Of Solid Polymers*, 3 ed., Wiley-VCH Verlag GmbH, Hoboken, NJ **2012**.
- [46] S. R. Cohen, E. Kalfon-Cohen, *Beilstein J. Nanotechnol.* **2013**, *4*, 815.
- [47] K. Friedemann, T. Corrales, M. Kappl, K. Landfester, D. Crespy, *Small* **2012**, *8*, 144.
- [48] F. Hang, D. Lu, S. W. Li, A. H. Barber, *Mater. Res. Soc.* **2009**, *1185*, 1185.
- [49] F. Müller-Plathe, W. F. van Gunsteren, *Polymer* **1997**, *38*, 2259.
- [50] D. T. W. Lin, C.-K. Chen, *Acta Mech.* **2004**, *173*, 181.
- [51] pyF4all Developers, pyDAMPF Repository examples 2021–2024, <https://github.com/pyF4all/pyDAMPF> (accessed: December 2023).
- [52] R. Garcia, *Amplitude Modulation Atomic Force Microscopy*, Wiley-VCH, Hoboken, NJ **2010**.
- [53] A. Calvimontes, *NPJ Microgravity* **2017**, *25*, 1.
- [54] H. V. Guzman, A. P. Perrino, R. Garcia, *ACS Nano* **2013**, *7*, 3198.
- [55] H. V. Guzman, R. Garcia, *Beilstein J. Nanotechnol.* **2013**, *4*, 852.
- [56] J. Domke, M. Radmacher, *Langmuir* **1998**, *14*, 3320.
- [57] X. Chen, R. Hughes, N. Mullin, R. J. Hawkins, I. Holen, N. J. Brown, J. K. Hobbs, *Biophys. J.* **2020**, *119*, 502.
- [58] T. L. Nguyen, E. R. Polanco, A. N. Patananan, T. A. Zangle, M. A. Teitell, *Sci. Rep.* **2020**, *10*, 7403.
- [59] C. H. Parvini, A. X. Cartagena-Rivera, S. D. Solares, *Commun. Biol.* **2022**, *5*, 17.
- [60] J. Legleiter, M. Park, B. Cusick, T. Kowalewski, *Proc. Natl. Acad. Sci. USA* **2006**, *103*, 4813.
- [61] M. Lee, W. Jhe, *Phys. Rev. Lett.* **2006**, *97*, 036104.
- [62] S. Hu, A. Raman, *Appl. Phys. Lett.* **2007**, *91*, 123106.
- [63] J. L. Aragonés, C. Vega, *J. Chem. Phys.* **2009**, *130*, 244504.
- [64] M. A. Gonzalez, A. Zaragoza, C. I. Lynch, M. S. P. Sansom, C. Valeriani, *J. Chem. Phys.* **2021**, *155*, 154502.
- [65] G. Gonella, E. H. G. Backus, Y. Nagata, D. J. Bonhuis, P. Loche, A. Schlaich, R. R. Netz, A. Kühnle, I. T. McCrum, M. T. M. Koper, M. Wolf, B. Winter, G. Meijer, R. K. Campen, M. Bonn, *Nat. Rev. Chem.* **2021**, *5*, 466.
- [66] L. Solhi, V. Guccini, K. Heise, I. Solala, E. Niinivaara, W. Xu, K. Mihhels, M. Kröger, Z. Meng, J. Wohler, H. Tao, E. D. Cranston, E. Kontturi, *Chem. Rev.* **2023**, *123*, 1925.
- [67] E. J. Curry, T. T. Le, R. Das, K. Ke, E. M. Santorella, D. Paul, M. T. Chorsi, K. T. M. Tran, J. Baroody, E. R. Borges, B. Ko, A. Golabchi, X. Xin, D. Rowe, L. Yue, J. Feng, M. D. Morales-Acosta, Q. Wu, I.-P. Chen, X. T. Cui, J. Pachter, T. D. Nguyen, *Proc. Natl. Acad. Sci. USA* **2020**, *117*, 214.
- [68] Y. Cheng, J. Xu, L. Li, P. Cai, Y. Li, Q. Jiang, W. Wang, Y. Cao, B. Xue, *Adv. Sci.* **2023**, *10*, 2207269.
- [69] R. Garcia, A. S. Paulo, *Appl. Phys. Lett.* **1999**, *60*, 4961.
- [70] T. Rodriguez, R. Garcia, *Appl. Phys. Lett.* **2002**, *80*, 1646.
- [71] S. O'Shea, M. Welland, *Langmuir* **1998**, *14*, 4186.
- [72] J. E. Sader, *J. Appl. Phys.* **1998**, *84*, 64.